ASTROMETRIC TECHNIQUES

M. M. COLAVITA
Jet Propulsion Laboratory, California Institute of Technology
4800 Oak Grove Dr., Pasadena, CA 91109 USA

interferometry

1. Astrometric Signatures

An exoplanet, while perhaps not visible from its direct radiation, can still make its presence known indirectly through its gravitational interaction with its parent star. As the planet and star revolve about the center of mass of the system, there will be a component of the star's motion both along and transverse to the line of sight. Velocity fluctuations along the line of sight can be detected using the radial velocity technique [1]; position fluctuations transverse to the line of sight can be detected using astrometry.

The astrometric signature is straightforward. Let θ be the amplitude of the (sinusoidal) astrometric signature. The angular signature is given by

$$\theta = \frac{m}{M}\frac{r}{L}, \tag{1}$$

where m and M are the planet and star masses, r is the planet's orbital radius, and L is the distance to the star. The amplitude θ is in arcsec for r in AU and L in pc. The standard example is the astrometric motion of the Sun caused by Jupiter($r = 5.2$ AU, $m = 1.0 \times 10^{-3} M$) as viewed from a distance of 10 pc: this gives a signature of 0.5 mas.

One feature of the astrometric technique is that it is sensitive to all orbital inclinations. Assume measurements in an orthogonal coordinate system on the sky. A system in a face-on orbit would yield identical signatures in each axis, while an edge-on system which yields no signature along one axis would provide a full signature along the other. This ability to measure the inclination allows determination of the planet-star mass ratio unambiguously.

Another feature of the astrometric signature is that it is inversely proportional to distance, and is thus is most sensitive to nearby targets. This can be contrasted with the radial-velocity technique, which while most sen-

TABLE 1. Astrometric signatures at 10 pc for stars of various spectral types (in μas)

	Spectral class			
Planet	F0	G2	K0	M0
Jupiter-mass, 11.9-y orbit	349	497	586	821
Saturn-mass, 11.9-y orbit	104	149	175	246
Uranus-mass, 11.9-y orbit	16	23	27	38
Earth-mass, 1-y orbit	0.21	0.30	0.36	0.50

sitive to nearby systems strictly from a detection-noise perspective (i.e., more photons), has a signature which is independent of distance [2].

We can also apply Kepler's law to write the astrometric signature in terms of the period P of the planet's orbit as

$$\theta = \frac{m}{L}\left(\frac{P}{M}\right)^{2/3}, \tag{2}$$

which is in arcsec for P in years and M and m in solar masses. Thus the astrometric technique is most sensitive to large orbital radii and long periods. In this sense it is complementary to radial-velocity techniques [1, 2], which are most sensitive to small orbital radii and short periods.

Figure 1 shows the motion of our Sun as viewed from a distance of 10 pc. The fundamental period is caused by Jupiter in its 11.9-y orbit, which introduces a component with a 500 μas amplitude. However, the presence of the other planets makes the signature more interesting, and a suitably accurate technique with an adequate time base could detect multiple planets from such data. Table 1 give the signatures for Jupiter, Saturn, and Uranus-mass objects in assumed 11.9-y orbits at a distance of 10 pc (see [1] for the expected astrometric signatures of the planets discovered through radial velocities). Thus, for the nearby sample, astrometric accuracies of 10–100 μas are required to do a comprehensive search for planets with masses down to that of Uranus. The table also gives the signature of an Earth-mass planet in a 1-y orbit; detection of such planets requires an astrometric accuracy of <1 μas.

Such astrometric measurements are challenging. The current state of the art for astrometry is $\sim$1 mas. This includes the results from the recent Hipparcos space mission [3], which measured thousands of stars to this accuracy, as well as parallaxes measured with ground-based CCD astrometry [4], and positions from the MAP instrument at Allegheny Observatory [5, 6]. Thus, current techniques fall short of what is required for a comprehensive search, and far short of what would be needed to detect an exoearth. However, application of the MAP and special-purpose CCD astrometry [7] on

Figure 1. The astrometric motion of the Sun as viewed from 10 pc.

large telescopes offers the promise of 100's of μas accuracy. Interferometry on the ground [8] offers the potential of 10's of μas accuracy. Interferometry in space with a mission such as SIM[9] is needed for accuracies < 10 μas.

2. Astrometric Techniques

Astrometric techniques in the visible and infrared use either single telescopes or interferometers. In principle, both instruments can be used on the ground or in space.

2.1. CCD ASTROMETRY

CCD astrometry for planet detection uses a CCD detector at the focus of a telescope to image the putative parent star plus nearby astrometric references. The field stars are used to calibrate the scale and geometry of the image plane [4]. For ground-based measurements, the atmosphere introduces errors attributable to differential chromatic refraction (DCR), and ultimately fundamental limits attributable to atmospheric turbulence. The USNO parallax program achieves mean accuracies of 1 mas using a CCD detector [4]. Pravdo & Shaklan [7] have examined a CCD astrometry system for planet detection, and estimate that an optimized system for use on a large telescope could achieve accuracies to $\sim$100 μas.

2.2. RONCHI RULING PHOTOMETER

As an alternative to CCD detectors, the Allegheny group [5] has used a Ronchi-ruling photometer to measure stellar positions. The approach uses a precision Ronchi ruling at the focus of the telescope. The ruling is translated in the telescope focal plane, imposing intensity modulation on the various stars in the field. Individual detectors for the target and reference stars collect the light which transmits through the Ronchi ruling; the phase shift of the modulated intensity of the various stars is the astrometric observable. The MAP (Multi-channel Astrometric Photometer) achieves accuracies of $\sim$1 mas at its current site; improved performance with an upgraded MAP to $\sim$100 μasis anticipated for planned observations at the Keck telescope (Gatewood97).

2.3. INTERFEROMETRIC ASTROMETRY

The rest of this paper will concentrate on interferometric techniques [10].

Interferometers have advantages over telescopes in several areas. In particular, resolution and sensitivity, viz. baseline and collecting area, can be set separately. With respect to photon noise (discussed later), the astrometric performance of an interferometer with baseline B and apertures of diameter d is similar to a telescope with diameter $\sim \sqrt{Bd}$. However, with respect to systematic errors, the interferometer has two advantages. The long baselines achievable with an interferometer reduce the angular effect of linear errors. Interferometers also have a simple geometry which can be accurately monitored to minimize systematic errors.

For astrometry, an optical interferometer can be looked at geometrically; the problem is identical to the case of a radio interferometer (see [11]). The delay x measured with the interferometer can be related to the interferometer baseline B and the star unit vector s as $x = B \cdot s$. Thus, measurements of delay in conjunction with knowledge of the baseline gives the angle of the star with respect to the baseline vector. This is shown schematically in Fig. 2.

The measurement can also be understood perhaps somewhat more intuitively. A stellar wavefront impinging on the interferometer at some angle arrives at one aperture delayed with respect to its arrival at the other aperture. This external delay is what we seek to measure. What the interferometer does is introduce a corresponding internal delay to match the external one; the internal delay is ordinarily introduced using an optical delay line. The internal delay has the advantage that it can be precisely monitored with a laser metrology system. In this case, the interference fringe is used as the measure of equality between the internal and external delays: when

Figure 2. Astrometry with an interferometer.

the fringe phase is equal to zero, the internal delay is a measure of the external delay.

In practice, the fringe phase can never be made exactly zero, and thus the delay is computed as

$$x = l + k^{-1}\phi, \tag{3}$$

where l is the laser-monitored internal delay, ϕ is the fringe phase, and k is the wavenumber of the interfering light.

3. Sources of Error

We can capture most aspects of the measurement problem by reducing it to 2-d and doing a small-angle approximation for sources near normal to the instrument, viz. $\theta \simeq x/B$. A trivial sensitivity analysis yields

$$\delta\theta = \frac{\delta l}{B} + k^{-1}\frac{\delta\phi}{B} - \frac{\delta B}{B}\theta. \tag{4}$$

The first term incorporates systematic errors in measuring the internal delay; the second term incorporates errors in measuring the fringe phase, including photon and detector noise; the third term incorporates errors in measurement or knowledge of the interferometer baseline.

3.1. SYSTEMATIC ERRORS

Astrometry at high accuracy is to a large extent about the control of systematic errors. The tolerances rapidly become very challenging. For example, the Space Interferometry Mission, SIM, has as one of its goals narrow-angle astrometry with an accuracy of 1 μas. With SIM's 10-m baseline, this corresponds to 50 pm length-measurement accuracy. As these errors are typically allocated among a number of terms, individual tolerances are smaller.

Laser metrology at the picometer level is a major technology area for SIM [12]. The types of effects which must be addressed include errors internal to the laser gauge itself, errors in the endpoints which define the length being measured, and errors attributable to alignment of the metrology beam to the endpoints. In addition, there are errors attributable to how well the path you can measure corresponds to the path you wish to measure. For example, sampling of the position of the center of a mirror with a laser beam is not necessarily representative of the mean position of the surface as would be illuminated by a stellar beam. While these measurements present challenges, the payoff is large, motivated by the high astrometric precision possible outside of the Earth's atmosphere.

Tolerances for ground interferometers are typically more modest, in part because of atmospheric limitations which preclude astrometry beyond a certain accuracy, and because the baseline lengths can be longer (at least with respect to first-generation space interferometers). For Keck Interferometer in astrometry mode using a 100-m baseline, 10 μas systematic accuracy requires a 5 nm total length error, which is closer to the current state-of-practice.

However, for both ground and space interferometers, some themes are common: longer baselines help given a fixed-level of linear metrology accuracy; differential measurements allows certain systematic errors to become common mode and drop out; measurements which can be performed in a switching mode allow a reduction of requirements on long-term thermal stability.

3.2. BASELINE ERRORS AND NARROW ANGLE ASTROMETRY

For general astrometry, we need to know the baseline vector to the same accuracy as the desired astrometry, that is, if we desire 10 μas astrometry with a 100-m baseline, we must know the baseline orientation to 10 μas, corresponding to knowledge of the vector components to $\sim$5 nm. However, planet detection is a special case in that it is fundamentally a narrow-angle problem, i.e., we can make measurements with respect to nearby astrometric references.

Equation 4 illustrates the difference between wide- and narrow-angle astrometry. For wide-angle astrometry, $\theta \sim 1$, leading to the intuitive result that the required fractional accuracy on the baseline is equal to the desired astrometric accuracy. However, for small fields, the requirement on baseline accuracy decreases: essentially, the baseline becomes more common mode to the differential measurement. For example, for a narrow-angle field of 20", the requirements on the baseline are reduced by a factor of 10^4.

3.3. RANDOM ERRORS - DETECTION NOISE

At some level, the ability to measure the fringe phase places a limit on the achievable accuracy. The error $\delta\phi$ in a phase measurement can be written

$$\delta\phi = (\mathrm{SNR}_\phi)^{-1}, \tag{5}$$

where

$$\mathrm{SNR}_\phi^2 \simeq \frac{1}{2}\frac{N^2V^2}{N+B+M\sigma^2}, \tag{6}$$

where N is the total photon count, B is the total background and dark count, σ^2 is the read-noise variance, and M is the number of reads needed to make the phase measurement.

The detection error shows up in the error expression, Eq. 4, reduced by the baseline. Thus, long baselines help by improving sensitivity for a given accuracy, or by reducing astrometric error for a given source brightness.

The SIM mission, observing in the visible, typically uses the photon-noise limit of this expression: $\mathrm{SNR}_\phi^2 \simeq (1/2)NV^2$. For ground-based interferometric astrometry in the infrared, the reference stars will ordinarily be faint and background limited, yielding $\mathrm{SNR}_\phi^2 \simeq (1/2)(N^2V^2/B)$.

3.4. RANDOM ERRORS - ATMOSPHERIC NOISE

For wide-angle optical astrometry on the ground, the ultimate limit to astrometric accuracy appears to be $\sim$1 mas, the goal of the USNO astrometric interferometer [13]. This limit is established by atmospheric turbulence which perturbs the position of a star. While techniques such as the two-color technique can help (and is incorporated into the number above), this limit appears fundamental, and thus wide-angle microarcsec astrometry remains the purview of space missions like SIM.

Narrow-angle astrometry presents a different problem: for a simultaneous measurement between two or more stars, the light rays through the atmosphere follow increasingly common paths as the angle between them is decreased. This effect can be quantified as shown in Fig. 3 (from [8]). With respect to narrow-angle astrometry, there are two key features: for small

Figure 3. Accuracy of narrow angle astrometry.

separations between stars, the errors are linearly dependent on the star separation, and nearly inversely dependent on the size of the instrument (the results are identical for either a telescope of diameter B or an interferometer with baseline B). This is in contrast to the case of larger separations, where the dependence on separation and instrument size is weaker. Thus, if it is possible to conduct a measurement with a long-baseline interferometer over a suitably small field, accuracies of tens of microarcsec are possible.

4. Implementing a Narrow-Angle Measurement

Exploiting the tens-of-microarcsec astrometric accuracy possible with a ground-based narrow-angle astrometric measurement requires the ability to utilize nearby reference stars. One approach to this problem uses a dual-star architecture [8], as shown in Fig. 4. It consists of a long-baseline interferometer with dual beam trains. The light at each aperture forms an image of the field containing the target star and the astrometric reference. A dual-star feed separates the light from the two stars into separate beams which feed separate interferometer beam combiners. These beam combiners are referenced with laser metrology to a common fiducial at each collector. The two beam combiners make simultaneous measurements of the delays for the two stars.

Over a small field, reference stars will invariably be faint, and ordinarily would not be usable by the interferometer. However, searching for exoplan-

Figure 4. Dual-star architecture.

ets is a special problem in that the target star is bright, and can serve as a phase reference. With phase referencing, the bright target star is used as a probe of the atmospheric turbulence within the isoplanatic patch of the target star. By compensating for the fringe motion of the target star with an optical delay line, the fringe motion of the faint astrometric reference star is frozen, allowing for long integration times which greatly increase sensitivity.

The radius of the isoplanatic patch increases with wavelength, and is 20–30 arcsec at 2.2 μm. With phase referencing and 1.5–2.0-m telescopes, astrometric references can be detected around most potential planetary targets.

Conducting a narrow-angle measurement with an architecture like that of Fig. 4 involves two steps. The first step is global astrometry using known reference stars to solve for the interferometer baseline. As discussed above, the required baseline precision for a narrow-angle measurement is much less than for a wide-angle measurement, and the accuracies available from these wide-angle measurements provide sufficient accuracy. (Strictly, if atmospherically-limited accuracy were always proportional to star separation, there would be difficulties with this step; however the break in the error dependence with large angles, as shown in Fig. 3, allows for a good baseline solution). There are some subtleties regarding the wide-angle baseline as thus solved and the narrow-angle baseline applicable to the science

measurement, and an auxiliary system may be required to tie these two baselines together.

The second step in the approach is to implement the measurement through chopping. In this approach, one interferometer beam combiner always tracks the target star. The other beam combiner switches repeatedly between the target star and the reference star. This "chopping" approach requires instrument stability only over the chop cycle (a similar approach would also be used for narrow-angle measurements with SIM). The use of even a low-resolution spectrometer in the fringe detector makes the ground-based measurements very insensitive to differential chromatic refraction.

In general, measurements on two orthogonal baselines are needed to detect systems with arbitrary inclinations. Measurements with respect to two reference stars are also desirable. With redundant measurements, astrometric noise in a reference star is in most cases separable from the desired (planetary) signature.

5. Astrometric interferometer projects

5.1. PALOMAR TESTBED INTERFEROMETER

The Palomar Testbed Interferometer (PTI) [14] was designed as a testbed for interferometry techniques applicable to other interferometers, especially the Keck Interferometer. It implements the dual-star architecture described above to develop the dual-star astrometry technique. PTI has been in operation since 1995 at Palomar Observatory. Recent astrometric observations on visual binaries have been used to examine the atmospheric limits predicted above and examine the long-term repeatability of the measurements. While this work is still proceeding, short-term accuracies have been achieved which are consistent with the atmospheric theory.

5.2. KECK INTERFEROMETER

The Keck Interferometer will combine the two 10-m Keck telescopes at Mauna Kea with 4 1.8-m outrigger telescopes as an interferometer [15]. The Keck Interferometer belongs to NASA's Origins [16] program. Science with the Keck Interferometer includes high-angular-resolution imaging [17], direct detection of hot Jupiters via a two-color phase-difference approach, measurement of the quantity of exozodiacal dust around nearby stars, and, apropos to this paper, interferometric astrometry using the 4 outriggers configured to provide orthogonal baselines [18]. Using this mode, a search for planets around several hundred nearby stars is planned. The Keck interferometer draws strongly on lessons learned from PTI. The planned development of the interferometer is over 5 years, starting in 1998, with the

astrometric program beginning after installation of the last of the outriggers in 2002.

The Very Large Telescope Interferometer (VLTI) is also considering instrumentation to allow for differential astrometry [19].

5.3. SPACE INTERFEROMETRY MISSION

The Space Interferometry Mission (SIM) [9] is the next major space mission in NASA's Origins Program after SIRTF, and is planned for a 2005 launch. SIM's primary goals are wide-angle astrometry to an accuracy of 4 μas to a limiting brightness of 20 mag, and synthesis imaging with a resolution of 10 mas. SIM uses 4 Michelson interferometers on a single structure with a maximum baseline of approximately 10 m. Several of these interferometers act as high-precision star trackers, stabilizing the interferometer to allow high-precision measurements with the other interferometers.

In addition to its wide-angle capability, SIM will also implement a narrow-angle astrometric capability with an accuracy of 1 μas. This is beyond the capability of ground-based techniques and is directed (through repeated measurements) at detecting planets down to several Earth masses around nearby stars.

6. Acknowledgments

The work reported here was performed at the Jet Propulsion Laboratory, California Institute of Technology, under a contract with the National Aeronautics and Space Administration.

References

1. Queloz, D. 1998, this proceedings
2. Marcy, G. W. & Butler, R. P. 1998, Ann. Rev. Astron. Astrophys. 36, 56
3. Perryman, M. A. C. et al. 1997, A&A, 323, L49
4. Monet, D. 1992, AJ 103, 638
5. Gatewood, G. D. 1987, Astron. J. 94, 213
6. Gatewood, G. D. et al. 1997, in Planets Beyond the Solar System, ASP Conf. Series Vol. 119, D. R. Soderblom, ed., 41
7. Pravdo, S. H. & Shaklan, S. B. 1996, ApJ 465, 264
8. Shao, M. & Colavita, M. M. 1992, A&A, 262, 353
9. Unwin, S., Boden, A., & Shao, M. 1997, in Space Technology and Applications International Forum, AIP Conf. Proc. 387 (AIP Press), 63; see also http://sim.jpl.nasa.gov
10. Shao, M. & Colavita, M. M. 1992, Ann. Rev. Astron. Astrophys, 30, 457
11. Thompson, A. R., Moran, J. M., Swensen, G. W., Jr. 1986, Interferometry and Synthesis in Radio Astronomy, Wiley, New York
12. Laskin, R. A. 1998, Proc. SPIE 3350, 654
13. Hutter, D. J., Elias, N. M., II, Hummel, C. A. 1998, Proc. SPIE 3350, 452
14. Colavita, M. M. et al. 1999, ApJ, in press

15. Colavita, M. M. et al. 1998, Proc. SPIE 3350, 776
16. http://origins.jpl.nasa.gov
17. Vasisht, G., Boden, A. F., Colavita, M. M., Crawford, S. L., Shao, M., van Belle, G. T., Wallace, J. K. 1998, Proc. SPIE 3350, 354
18. van Belle, G. T., Boden, A. F., Colavita, M. M., Shao, M., Vasisht, G., Wallace, J. K. 1998, Proc. SPIE 3350, 362
19. Mariotti, J.-M. et al. 1998, Proc. SPIE 3350, 800

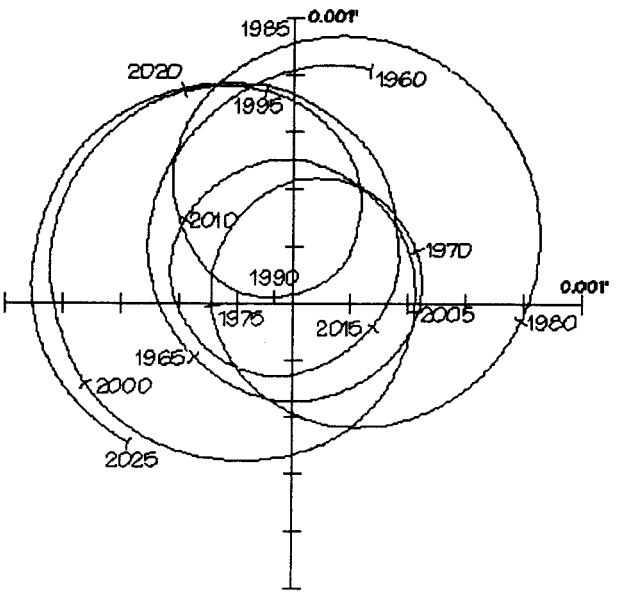
0.001'
1985
2020
1960
1995
2010
1970
1990
0.001'
1975
2015
2005
1980
1965
2000
2025

Fig 1

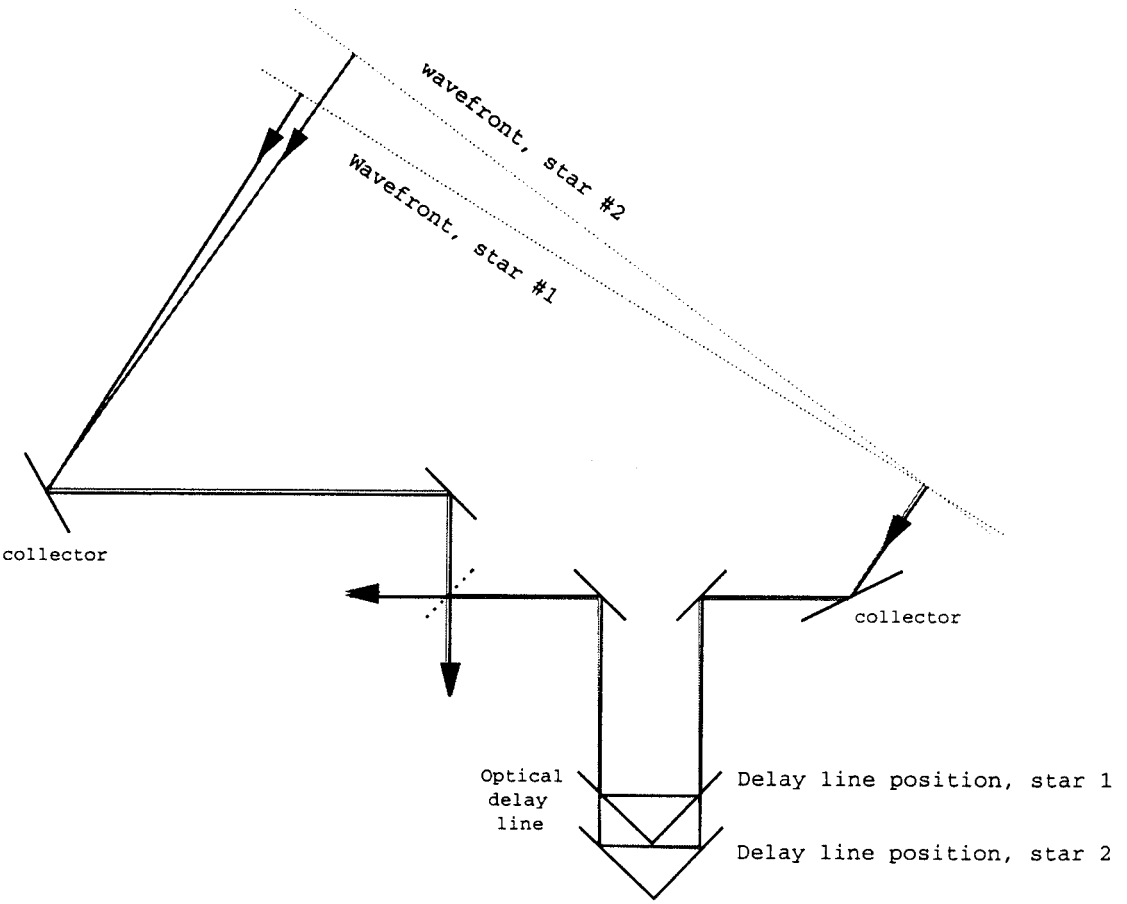
wavefront, star #2
Wavefront, star #1
collector
collector
Optical
delay
line
Delay line position, star 1
Delay line position, star 2

FIG 2

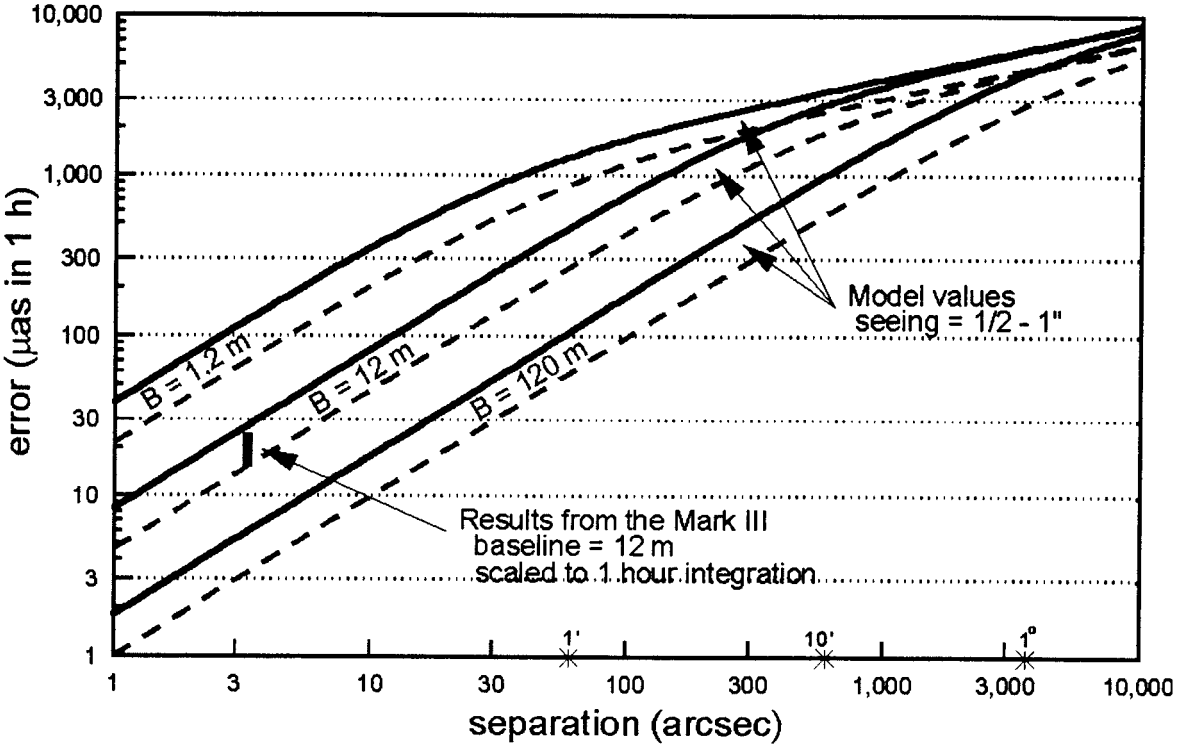
10,000
3,000
1,000
300
100
30
10
3
1
error (μas in 1 h)
B = 1.2 m
B = 12 m
B = 120 m
Model values
seeing = 1/2 - 1"
Results from the Mark III
baseline = 12 m
scaled to 1 hour integration
1'
10'
1°
1
3
10
30
100
300
1,000
3,000
10,000
separation (arcsec)

Fig 3

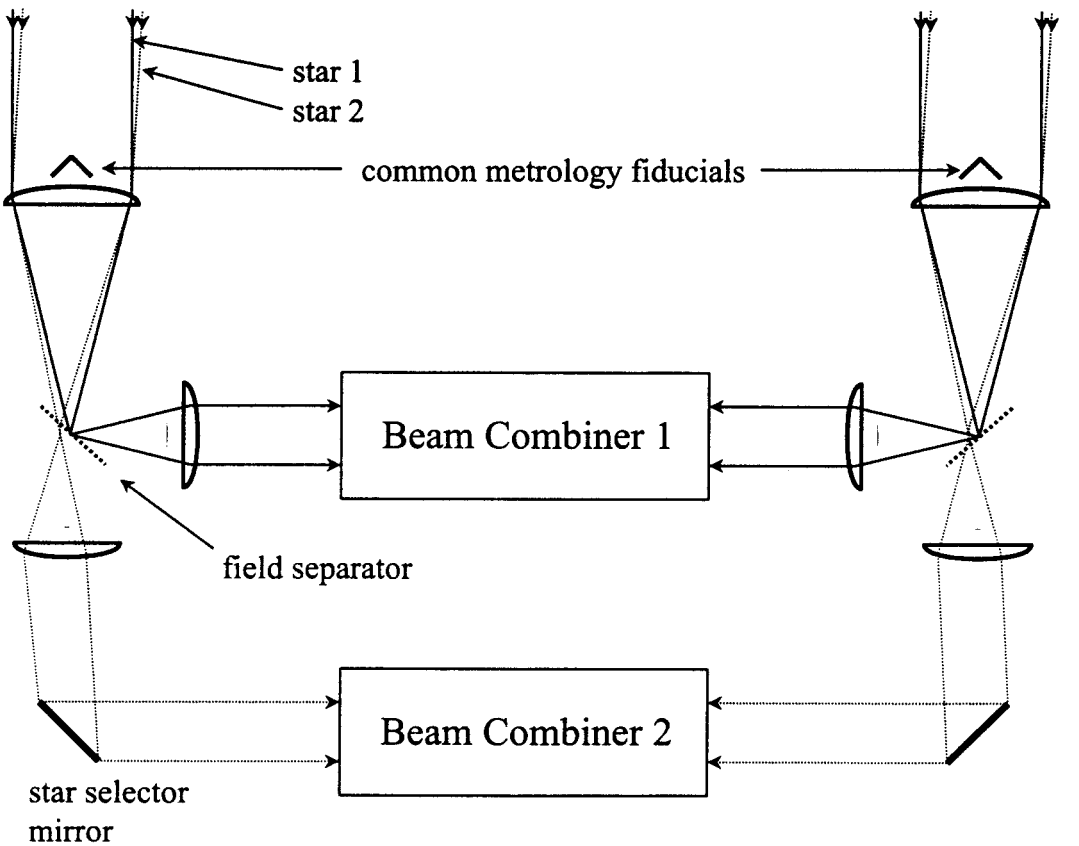
star 1
star 2
common metrology fiducials
Beam Combiner 1
field separator
Beam Combiner 2
star selector
mirror

Fig 4